Nanoscale

PAPER

View Article Online
View Journal | View Issue

Cite this: *Nanoscale*, 2017, **9**, 16005

In-site encapsulating gold "nanowires" into hemin-coupled protein scaffolds through biomimetic assembly towards the nanocomposites with strong catalysis, electrocatalysis, and fluorescence properties†

Shuai Li,‡ Liyan Zhang,‡ Yao Jiang, Shuyun Zhu, Xiaoxia Lv, Zhiqiang Duan and Hua Wang *

An efficient and green biomimetic assembly protocol was developed for the fabrication of multifunctional nanocomposites by mimicking the configuration of natural protein enzymes. Bovine serum albumin (BSA) as the protein model was first split to produce the disassembled BSA (dBSA) of linear polymer and then coupled with catalytic Hemin (Hem). The yielded dBSA-Hem scaffolds were utilized to in-site encapsulate gold nanoclusters (AuNCs) through biominerization, yielding the dBSA-Hem-AuNCs. It was discovered that the nanocomposites could display the well-defined composition and spheric morphology. In particular, they could exhibit unexpectedly strong catalysis, electrocatalysis, and fluorescence properties, in which the biominerized AuNCs would act as fluorescence sources and "nanowires" for promoting the electron-transfer of the catalytic nanocomposites. Colorimetric investigations show that the developed enzyme mimics could present peroxidase-like catalysis activities comparable to natural horseradish peroxidase. In addition, they could facilitate the direct electrocatalysis for H_2O_2 at concentrations as low as 0.40 μM. Moreover, strong red fluorescence of AuNCs in nanocomposites could be expected for the fluorimetric analysis of H_2O_2 with linear concentrations ranging from 50 nM to 100 μM. Such a biomimetic assembly route may open a new door toward the preparation of diverse nanocomposites with multifunctional catalysis and fluorescence, thus promising extensive applications of catalysis and detection in the chemical, environmental, and biomedical fields.

Received 8th July 2017,
Accepted 27th September 2017

DOI: 10.1039/c7nr04945e

rsc.li/nanoscale

Introduction

Natural enzymes, particularly protein enzymes, with high catalysis efficiency and specificities have been widely applied in different catalysis fields. However, they may suffer from some disadvantages such as cost-ineffectiveness, storage difficulty, easy denaturation, and environment-affected catalysis activities.[1] Aiming to overcome these drawbacks of natural enzymes, huge efforts have alternatively contributed to the development of artificial enzyme mimics,[2] such as heme,[3,4] hemeatin,[5] cyclodextrin,[6] and porphyrin.[7,8] Herein, heme, which generally converts to hemin (Hem) *in vitro*, is well established to be the redox active site for heme-containing proteins like hemoglobin and horseradish peroxidase (HRP).[9–11] However, the direct applications of cheap heme or Hem as a catalyst can be challenged by some limitations such as sparing solubility in water, destructibility in oxidizing media, and aqueous molecular aggregation forming catalytically inactive dimers.[12] In addition, the catalysis environments of Hem are very different from those of most peroxidases like HRP. For example, the optimum catalysis reaction of Hem occurs in hash alkaline solution (about pH 11),[13] much higher than that of HRP (pH 5.8), of which the applications in the neutral biological systems can be greatly limited.

The past few decades have witnessed the rapid development of nanomaterials and nanocomposites,[14,15] particularly those exhibiting peroxidase-like catalysis activities, such as Fe_3O_4 nanoparticles,[14] cerium oxide nanoparticles,[16,17] silver nanoparticles,[18] graphene oxide nanosheets,[19] Fe_3O_4 nanocomposites,[20] Pt nanocomposites,[21] and carbon nanotubes.[22]

Institute of Medicine and Materials Applied Technologies, College of Chemistry and Chemical Engineering, Qufu Normal University, Qufu City, Shandong Province 273165, P. R. China. E-mail: huawangqfnu@126.com; http://wang.qfnu.edu.cn; Fax: +865374456306; Tel: +86 5374456306

†Electronic supplementary information (ESI) available. See DOI: 10.1039/c7nr04945e

‡These authors contributed equally.

However, numerous disadvantages should be addressed before they could be applied on a large scale, such as low catalytic efficiency, biological toxicity, limited selectivity, and unclear mechanism.[2,23,24] Moreover, the catalysis performance of metal nanomaterials, such as gold nanomaterials, could substantially depend on their sizes, known as the "size effect".[25–28] As a result, gold nanoclusters (AuNCs) with small sizes (less than 5.0 nm) have been widely prepared and applied.[29–31] Notably, they could present the additional advantages of high stability and biocompatibility for biomedical applications.[32–34] Although AuNCs as enzyme mimics have still been limited by their low catalysis activity for direct applications, their catalysis activity could be improved with some enzyme-like modulation materials such as graphene oxide.[35] Moreover, the protein-templated preparation strategy has recently emerged for the synthesis of functional nanomaterials under mild conditions.[36,37] For example, bovine serum albumin (BSA) was utilized as the protein scaffold to template the synthesis of AuNCs by way of biominerization;[38,39] however, this method entailed very high protein dosages.

Inspired by the structure and configuration of natural protein enzymes, in the present study, intact BSA was alternatively split by reduction to yield the linear polymer of disassembled BSA (dBSA) to be coupled with Hem extracted from the catalysis-active centers of heme-containing proteins like hemoglobin. The obtained dBSA-Hem scaffolds, which could serve as stabilizer and reduction agents[40] with the exposed 35 cysteine residues,[41] were utilized for the in-site encapsulation of AuNCs by biominerization, followed by the reassembly of the protein scaffolds of dBSA. To our surprise, the resulting dBSA-Hem-AuNCs nanocomposites exhibited multifunctional properties of strong catalysis, electrocatalysis, and fluorescence, in which the formed AuNCs would act as fluorescence sources and "nanowires" for promoting the electron-transfer towards improved catalysis of the nanocomposites. The HRP-like catalysis activities of the obtained dBSA-Hem-AuNCs were systematically investigated in catalyzing the typical chromogenic reactions of 3,3′,5,5′-tetramethyl benzidine (TMB) and H_2O_2 together with the calculated steady-state kinetic parameters. Moreover, the electrocatalysis performance of the enzyme mimetics was confirmed in sensing H_2O_2. In addition, the developed nanocomposites with strong red fluorescence of AuNCs were employed for the fluorimetric assay of H_2O_2 by H_2O_2-induced fluorescence quenching. To the best of our knowledge, this is the first success on the bio-inspired assembly of nanocomposites with multifunctional catalysis and fluorescence by mimicking the structure and configuration of natural protein enzymes with catalysis active centers-coupled protein scaffolds and biominerized gold "nanowires".

Results and discussion

Synthesis and characterization of dBSA-Hem-AuNCs

It is well recognized that native Hem, which is generally extracted from the catalysis-active centers of heme-containing proteins like hemoglobin, could display substantially low catalysis activity, as compared to natural peroxidases like HRP. By mimicking the configuration of natural protein enzymes, in the present study, the multifunctional nanocomposites were fabricated by the biomimetic assembly procedure as schematically shown in Scheme 1. Typically, intact BSA was denaturated and disassembled by using urea and dithiothreitol (DTT) to produce the linear polymer of dBSA with exposed 35 cysteine residues containing amine groups,[41] and then coupled with the catalytic Hem with carboxyl groups (Hem-COOH) by the cross-linking chemistry. The as-obtained dBSA-Hem scaffolds were first encapsulated in site with AuNCs by biominerization, and simultaneously reassembled to yield the dBSA-Hem-AuNCs nanocomposites through the interaction between their cysteine residues with thiols and encapsulated AuNCs. Herein, the dBSA-Hem scaffolds with some functional groups (*e.g.*, amine, carboxyl, and thiol groups) could act as stabilizer and reducing agents for the gold biominerization at a low protein concentration of dBSA (*i.e.*, 2.0 mg mL^{-1}) in contrast to that of intact BSA (*i.e.*, 50 mg mL^{-1}) reported elsewhere for gold biominerization.[36] In particular, AuNCs could be encapsulated into the dBSA-Hem scaffolds acting as "nanowires" for promoting the electron-transfer of the nanocomposites towards enhanced catalysis. Strong red fluorescence of AuNCs could also be expected for the resulting nanocomposites. Therefore, the as-prepared dBSA-Hem-AuNCs could feature multiple functions of peroxidase-like catalysis, electrocatalysis, and fluorescence properties and shows promise in the catalysis and florescence analysis applications demonstrated in the subsequent sections.

To figure out the potential roles of dBSA and Hem in the formation of AuNCs, dBSA and Hem were separately employed to synthesize AuNCs, according to the procedure described in our recent report.[42] Interestingly, both dBSA and Hem could

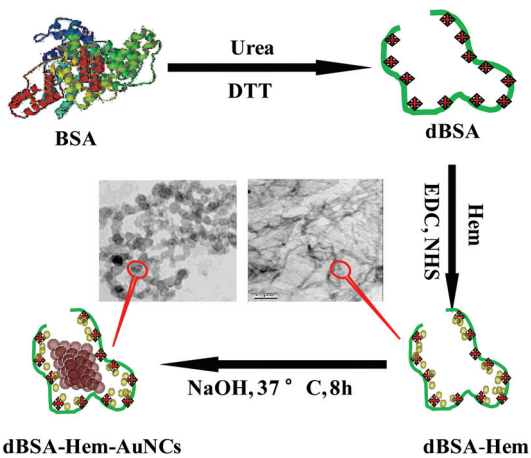

Scheme 1 Schematic illustration of the biomimetic assembly principle and procedure of the multifunctional dBSA-Hem-AuNCs nanocomposites, including the BSA disassembly for dBSA, Hem coupling for dBSA-Hem scaffolds, in-site biominerization of AuNCs, and protein scaffold reassembly by using BSA, Hem-COOH, and $HAuCl_4$.

serve as reducing agents in yielding AuNCs but showed different particle sizes, presumably due to the existence of some reductive groups like thiol and pyrrole in dBSA and Hem, respectively. Moreover, Hem could be covalently coupled onto the linear polymer of dBSA to obtain the dBSA-Hem, showing a filamentous scaffold structure as shown in the TEM image (Fig. 1A). In particular, the enhanced reduction could thus be expected in the in-site encapsulation of AuNCs and scaffold reassembly to form stable dBSA-Hem-AuNCs. Fig. 1B manifests the TEM image of the resulting dBSA-Hem-AuNCs. Accordingly, the prepared nanocomposites can illustrate the well-defined composition and spherical morphology, which were mostly aggregated with an average particle size of about 5.5 nm, as more clearly shown in the amplified TEM view (Fig. 1C), which is basically consistent with the protein size of BSA.[43] Fig. 1D displays the further amplified TEM image of the nanocomposites that were furnished with gold signatures showing the apparent crystalline lattices, of which AuNCs (less than 2.0 nm in diameter) were encapsulated in the dBSA scaffold as-reassembled. Moreover, UV-vis spectra of dBSA-Hem-AuNCs were measured by comparing to those of native Hem and dBSA (Fig. 2A). It could be noted that the dBSA-Hem-AuNCs could display two absorption peaks at 280 nm and 397 nm, which are assigned to dBSA and Hem, respectively, indicating that they could exist in the nanocomposites. However, there is no absorption peak in the range of 500–550 nm, which can belong to gold nanoparticles with large particle sizes, implying the formation of small AuNCs in the dBSA-Hem-AuNCs. Therefore, the data above indicate that the dBSA-Hem-AuNCs nanocomposites were successfully synthesized through mimicking the configuration of natural protein enzymes, of which the catalysis active centers-coupled protein scaffolds were produced for in-site biominerization of gold "nanowires".

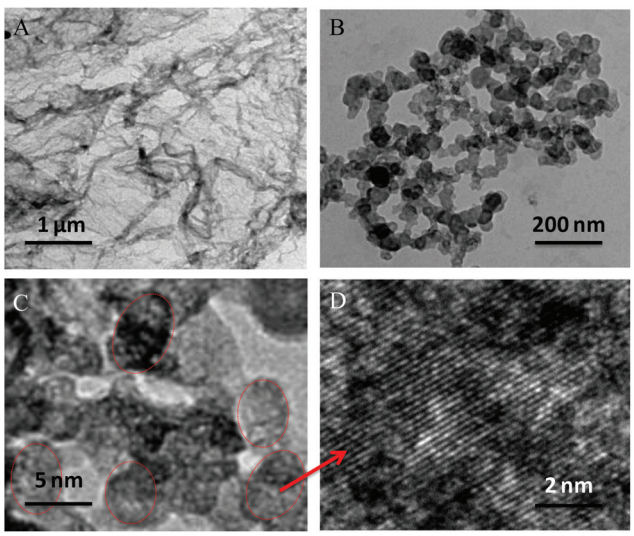

Fig. 1 TEM images of (A) dBSA-Hem scaffolds, (B) dBSA-Hem-AuNCs in low magnitude view, and (C, D) dBSA-Hem-AuNCs in the magnitude-amplified views.

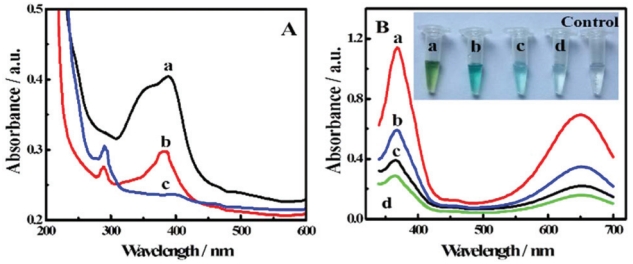

Fig. 2 (A) UV-vis spectra of (a) Hem, (b) dBSA-Hem-AuNCs, and (c) dBSA. (B) Typical absorption curves of the reaction products of the TMB–H_2O_2 reactions catalyzed separately by (a) dBSA-Hem-AuNCs, (b) Hem-AuNCs, (c) Hem, and (d) AuNCs. The catalytic TMB–H_2O_2 reactions were monitored with corresponding photographs (insert).

Colorimetric investigations of peroxidase-like catalysis activities of dBSA-Hem-AuNCs

The peroxidase-like catalysis properties of dBSA-Hem-AuNCs were investigated by colorimetric tests using the TMB–H_2O_2 reactions. Fig. 2B shows the results detailing the comparison of catalysis activities among dBSA-Hem-AuNCs, Hem-AuNCs, Hem (each containing Hem of similar concentration), and AuNCs. The UV-vis absorbance peaks of the TMB–H_2O_2 products were monitored at 375 nm and 652 nm. Clearly, the dBSA-Hem-AuNCs could display much stronger catalysis performances than either of Hem-AuNCs, Hem, and AuNCs. Herein, the enhanced catalysis activity of dBSA-Hem-AuNCs was thought to result mainly from Hem, whose catalysis activity was dramatically enhanced by biominerized gold "nanowires" that would accelerate the electron transfer involved. In addition, the encapsulated AuNCs with the "size effect"-dependent catalysis[25] could to some degree contribute to the catalysis of dBSA-Hem-AuNCs. Besides, the dBSA-Hem scaffolds not only facilitate the formation of biominerized AuNCs but also provide the desirable catalysis micro-environments for improving the catalysis of the as-assembled dBSA-Hem-AuNCs.

To further characterize the catalysis activities of dBSA-Hem-AuNCs, kinetic investigations were conducted and compared with those of Hem-AuNCs and native Hem. The Michaelis constant (K_m) and maximal reaction velocity (V_m) values were calculated by the typical Lineweaver–Burk double reciprocal curves (Fig. S1A and B†) and summarized in Table S1.† It could be observed that the apparent K_m of dBSA-Hem-AuNCs for TMB (0.518 mM) is significantly lower than those of Hem-AuNCs (4.80 mM) and Hem (5.06 mM), so was its maximal reaction velocity. Moreover, dBSA-Hem-AuNCs could present much lower K_m than the others. In particular, the K_m of dBSA-Hem-AuNCs for H_2O_2 is surprisingly nearly six times lower than that of HRP as reported elsewhere,[14] indicating the higher catalysis affinity to the oxidizing substrates.

The possible catalysis mechanism of dBSA-Hem-AuNCs in catalyzing TMB–H_2O_2 reactions was further explored. The double reciprocal plots of initial velocity against three fixed concentrations of one substrate were obtained over a range of concentrations of the second substrate (Fig. S1C and D†). It is

found that the parallel lines were obtained for both TMB and H_2O_2 substrates with three concentrations, indicating that the characteristic catalysis of dBSA-Hem-AuNCs should feature a ping-pong type mechanism as reported elsewhere for other Hem-existing enzymes such as HRP.[14] Furthermore, Hem could play a vital role in the catalysis behavior of dBSA-Hem-AuNCs. In addition, it is well established that the catalytic activities of peroxidases like HRP depends on the pH values, temperature, and ionic strengths.[44,45] The main catalysis reaction conditions of dBSA-Hem-AuNCs were studied with the results shown in Fig. S2.† Accordingly, the optimal catalysis conditions for the as-prepared nanocomposites are found to be close to the physiological conditions (37 °C at pH 6.0) except for NaCl of 18 mg mL^{-1}. Besides, the storage stability of dBSA-Hemin-AuNCs was also studied (Fig. S2D†), showing no significant changes in the catalytic activities of the nanocomposites stored for the long term (up to 14 weeks).

Moreover, colorimetric assays using dBSA-Hem-AuNCs were conducted for probing H_2O_2. Fig. 3A describes the comparison of H_2O_2 concentration-dependent colorimetric responses among dBSA-Hem-AuNCs, Hem-AuNCs, and Hem. As expected, the developed dBSA-Hem-AuNCs displayed the best responses to H_2O_2 using the optimal nanocomposite concentration of 3.0 μg mL^{-1} (Fig. S5E†). Remarkably, it was found that the enzyme mimetics could tolerate the toxic H_2O_2 with the concentration up to 250 mM, whose capacity is much stronger than that of HRP.[46] Fig. 3B shows the concentration–response curve of dBSA-Hem-AuNCs for H_2O_2. It could be observed that H_2O_2 can be detected in the concentrations linearly ranging from 5.0 μM to 0.21 mM, with a high correlation coefficient (R^2 = 0.9843). A detection limit of 1.2 μM is estimated by the 3σ rule, which is also lower than that of HRP reported elsewhere (20 μM).[47]

Electrochemical studies on the electrocatalysis activities of dBSA-Hem-AuNCs

The electrocatalysis performances of dBSA-Hem-AuNCs as enzyme mimetics for H_2O_2 were evaluated comparably. Fig. 4

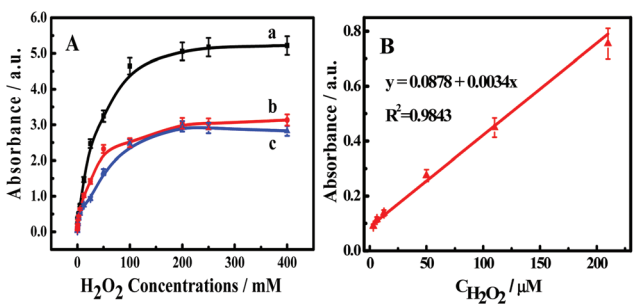

Fig. 3 (A) Colorimetric comparison of H_2O_2 concentration-dependent responses among (a) dBSA-Hem-AuNCs, (b) Hem-AuNCs, and (c) Hem, each containing 2.0 μg mL^{-1} Hem, using 0.69 mM TMB as the substrate. (B) The calibration curve of dBSA-Hem-AuNCs-based colorimetric assays with the absorbance values *versus* different H_2O_2 concentrations ranging from 5.0 μM to 0.21 mM.

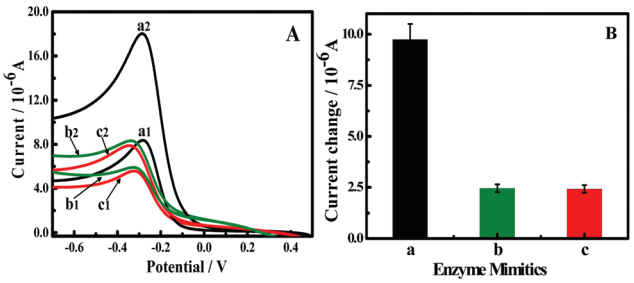

Fig. 4 (A) Electrochemical LSV responses of the electrodes modified separately with (a) dBSA-Hem-AuNCs, (b) Hem-AuNCs, and (c) Hem before (lines a1, b1, and c1) and after (lines a2, b2, and c2) the addition of 0.50 mM H_2O_2, corresponding to (B) the differences of current responses of these enzyme mimics between before and after the additions of H_2O_2.

manifests the electrochemical LSV responses of the dBSA-Hem-AuNCs modified electrode before and after adding H_2O_2 (line a), taking the ones with Hem-AuNCs (line b) and Hem (line c) for the comparison. As shown in Fig. 4A, the peak potential of LSV responses of the dBSA-Hem-AuNCs electrode peaked at −0.28 V, which is lower than those of the Hem and Hem-AuNCs electrodes both peaking at −0.32 V. Accordingly, a more efficient electron-transfer between the active centers of dBSA-Hem-AuNCs and the electrode surfaces could thus be expected, presumably due to the encapsulation of AuNCs that could act as "nanowires" to promote the electronic shuttling from their catalytic active centers to the electrode surfaces. In particular, much larger current responses to H_2O_2 could thus be achieved for the dBSA-Hem-AuNCs electrode (Fig. 4A, the upper line a). As shown in Fig. 4B, the current difference of the nanocomposites modified electrode is much higher than those of Hem and Hem-AuNCs modified electrodes, resulting in much higher H_2O_2 electrocatalysis.

Furthermore, a scan rate study was performed for the dBSA-Hem-AuNCs modified electrode with the electrochemical CVs over the potentials scanning from 25 to 200 mV s^{-1} (Fig. S3A†). It could be observed that the peak currents gradually increase as the scan rates increase, showing a linear relationship between scan rates and peak currents (Fig. S3B†). A surface controlled electron transfer could thereby occur for the dBSA-Hem-AuNCs modified electrodes. In particular, the shape of the H_2O_2 reduction peaks was well-retained for the developed electrode even on conducting the electrochemical CVs 20 times with continuous addition of H_2O_2. In contrast, the Hem and Hem-AuNCs modified electrodes survived for no more than 10 times (data not shown). Furthermore, the electrocatalysis stability was comparably studied for the dBSA-Hem-AuNCs modified electrodes by performing CVs of 100 consecutive cycles at a scan rate of 50 mV s^{-1} (Fig. S4†). It can be seen from Fig. S4a† that the developed electrodes could maintain better shape of reduction peak, higher reduction peak current, and lower peak potential when compared with these electrodes modified separately with Hem-AuNCs (Fig. S4b†) and Hem (Fig. S4c†). In addition, the nano-

composite dosage-depending responses for the H_2O_2 electroanalysis were measured, showing an optimal concentration of 2.0 μg mL^{-1} (Fig. S5F†). The above results indicate that the dBSA-Hem-AuNCs modified electrodes could achieve much higher electrocatalysis and stability in sensing H_2O_2.

The electrocatalysis performances of the dBSA-Hem-AuNCs electrodes were further investigated for sensing H_2O_2 (Fig. 5). When H_2O_2 was added at a step of 0.50 mM, a rapid increase in the reduction peak current was observed reaching 95% of the steady-state current within 5 s. In particular, the obtained current responses could increase linearly with the increasing concentrations of H_2O_2 (Fig. 5A) with the corresponding CVs (Fig. 5A, insert). A calibration curve was thereby obtained for the analysis of H_2O_2 for the dBSA-Hem-AuNCs electrodes (Fig. 5B). Accordingly, H_2O_2 could be detected with concentrations ranging from 2.0 μM to 2.2 mM, with a detection limit of about 0.40 μM (by 3σ rule), which is comparable to those of the H_2O_2 electroanalysis documented previously using the HRP modified electrodes (*i.e.*, 0.42 μM and 9.0 μM).[48–53] Therefore, the developed dBSA-Hem-AuNCs electrodes can allow for the electroanalysis of H_2O_2 with high detection sensitivity.

Fluorimetric evaluation for dBSA-Hem-AuNCs with fluorescence

It was discovered that the as-prepared dBSA-Hem-AuNCs could emit the blue and red fluorescence peaking at 437–460 nm and 625 nm (Fig. 6A **a**), respectively, which are similar to those of AuNCs alternatively synthesized using HRP templates.[54] Herein, the red fluorescence of dBSA-Hem-AuNCs at 625 nm could originate from small AuNCs so encapsulated. As for the blue fluorescence peak at 437–460 nm, it could come from the dBSA-Hem scaffolds with some aromatic side groups of some amino acid residues (*i.e.*, tryptophan, tyrosine, and phenylalanine),[55] as comparably confirmed in Fig. 6A **c**. Interestingly, the addition of H_2O_2 could induce the fluorescence of the nanocomposites to be quenched and enhanced at 625 nm and 460 nm, respectively (Fig. 6A **b**). Fig. 6B shows that H_2O_2 could quench the fluorescence of dBSA-Hem-AuNCs till it completely disappeared. In particular, the quenching degrees of the fluorescence of dBSA-Hem-AuNCs could depend on the amounts of H_2O_2, as visually witnessed by the corresponding photographs in Fig. 6C. Moreover, the effects of reaction temperature, pH values, and nanocomposite amounts on the fluorescence responses were investigated (Fig. S5†), showing the optimal conditions of pH 7.0 at 25 °C using nanocomposites of 1.0 μg mL^{-1}. In addition, it was found that the H_2O_2-induced fluorescence quenching of dBSA-Hem-AuNCs could be completed within 7 min (Fig. S5C†). Accordingly, a fluorimetric analysis method was developed to probe H_2O_2 using the as-prepared nanocomposites (Fig. 7A and B). It was observed that the fluorescence peak ratios of F_{625}/F_{460} could decrease linearly with the increasing H_2O_2 concentrations ranging from 50 nM to 100 μM. The limit of detection for H_2O_2 is about 15 nM as estimated by 3σ rule, which is lower than those of the fluorimetric H_2O_2 analysis using AuNCs prepared by HRP templates (LOD = 30 nM).[54,56,57] Therefore, the unique red fluorescence characteristics of dBSA-Hem-AuNCs could not only facilitate the sensitive fluorimetric analysis for H_2O_2 but also show promise in potential applications for the fluorescence imaging of H_2O_2 in biological samples.

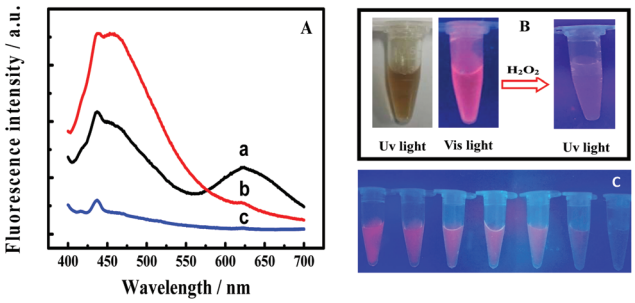

Fig. 6 (A) Fluorescence spectra of dBSA-Hem-AuNCs in the (a) absence and (b) presence of 50 mM H_2O_2, with (c) dBSA-Hem scaffolds as the control. (B) The photographs of dBSA-Hem-AuNCs under visible light and UV light (ex 380 nm) in the (left) absence and (right) presence of 50 mM H_2O_2. (C) The physical map of fluorescence responses of dBSA-Hem-AuNCs to H_2O_2 with concentrations ranging from 50 nM to 100 μM.

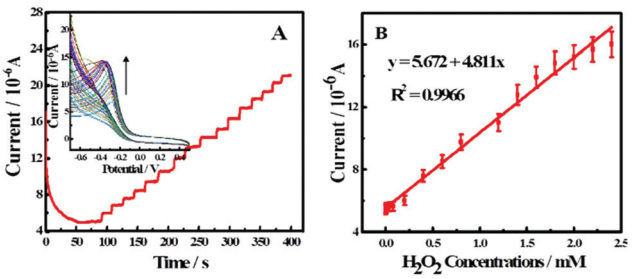

Fig. 5 (A) Amperometric responses recorded at the electrodes modified with dBSA-Hem-AuNCs to the successive additions of H_2O_2 at a step of 0.50 mM at a potential of −0.30 V with corresponding CVs (insert); (B) the calibration curve of the current responses *versus* different H_2O_2 concentrations ranging from 2.0 μM to 2.2 mM.

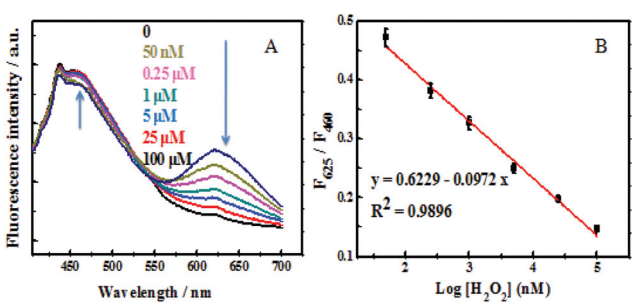

Fig. 7 (A) Fluorescence responses of dBSA-Hem-AuNCs to H_2O_2 with the concentrations ranging from 50 nM to 100 μM. (B) The calibration curve with the fluorescence ratios [F_{625}/F_{460}] *versus* the logarithmic concentrations of H_2O_2.

Conclusions

In the present study, multifunctional nanocomposites have been prepared for the first time by way of the biomimetic assembly through mimicking the configuration of natural protein enzymes. Compared to native Hem or Hem-AuNCs, the prepared nanocomposites of dBSA-Hem-AuNCs could present dramatically enhanced catalysis and electrocatalysis performances as evidenced by the colorimetric and electroanalytic H_2O_2 assays. In addition, steady-state kinetic studies indicate that dBSA-Hem-AuNCs could display much better affinity to the catalyzing reaction substrates, of which the Michaelis constants are even lower than those of natural peroxidases like HRP. Herein, the protein scaffolds of dBSA-Hem could facilitate the formation of AuNCs by biominerization and provide the catalysis micro-environments for the resulting nanocomposites. Moreover, the encapsulated AuNCs acting as "nanowires" inside dBSA-Hem-AuNCs could boost the electron-transfer towards the enhanced catalysis of nanocomposites. Besides, strong red fluorescence of AuNCs could be additionally expected for the dBSA-Hem-AuNCs. Therefore, the developed nanocomposites feature peroxidase-like catalysis and red fluorescence properties, which should find wide applications in catalysis-based sensing and fluorimetric analysis. In particular, such a facile and efficient biomimetic assembly route may open a new way toward fabrication of diverse nanocomposites with multifunctional catalysis and florescence properties. However, more efforts need to be made to translate the fundamental phenomenon and potential scientific mechanism before it can be practically applied on a large scale.

Conflicts of interest

There are no conflicts to declare.

Acknowledgements

This study is supported by the National Natural Science Foundations of China (no. 21675099, 21375075, and 21405094), the Natural Science Foundation of Shandong Province (no. ZR2013BQ018), and the Taishan Scholar Foundation of Shandong Province, P. R. China.

Notes and references

1 J. Xie, X. Zhang, H. Wang, H. Zheng and Y. Huang, *Trends Anal. Chem.*, 2012, **39**, 114–129.
2 H. Wei and E. Wang, *Chem. Soc. Rev.*, 2013, **42**, 6060–6093.
3 Q. Zhu, F. Liu, J. Xu, W. Su and J. Huang, *Anal. Chem.*, 1998, **362**, 537–540.
4 L. Fruk and C. M. Niemeyer, *Angew. Chem., Int. Ed.*, 2005, **44**, 2603–2606.
5 G. Zhang and P. K. Dasgupta, *Anal. Chem.*, 1992, **64**, 517–522.
6 Z. Liu, R. Cai, L. Mao, H. Huang and W. Ma, *Analyst*, 1999, **124**, 173–176.
7 R. P. Bonarlaw and J. K. M. Sanders, *J. Am. Chem. Soc.*, 1995, **117**, 259–271.
8 Y. Ci, Y. Zheng, J. Tie and W. Chang, *Anal. Chim. Acta*, 1993, **282**, 695–701.
9 T. Xue, S. Jiang, Y. Qu, Q. Su, R. Cheng, B. Du, C. Chiu, R. Kaner, Y. Huang and X. Duan, *Angew. Chem., Int. Ed.*, 2012, **51**, 3822–3825.
10 Y. Li, H. Liu, Z. Dong, W. Chang and Y. Ci, *Microchem. J.*, 1996, **53**, 428–436.
11 Y. Li and A. Townshend, *Anal. Chim. Acta*, 1997, **340**, 159–168.
12 A. M. Toader and E. Volanschi, *Rev. Roum. Chim.*, 2007, **52**, 159–167.
13 Y. Li, N. He, X. Wang, W. Chang and Y. Ci, *Analyst*, 1998, **123**, 359–364.
14 L. Gao, J. Zhuang, L. Nie, J. Zhang, Y. Zhang, N. Gu, T. Wang, J. Feng, D. Yang, S. Perrett and X. Yan, *Nat. Nanotechnol.*, 2007, **2**, 577–584.
15 A. Chen and S. Chatterjee, *Chem. Soc. Rev.*, 2013, **42**, 5425–5438.
16 T. Pirmohamed, J. M. Dowding, S. Singh, B. Wasserman, E. Heckert, A. S. Karakoti, J. E. S. King, S. Seal and W. T. Self, *Chem. Commun.*, 2010, **46**, 2736–2738.
17 A. Asati, S. Santra, C. Kaittanis, S. Nath and J. M. Perez, *Angew. Chem., Int. Ed.*, 2009, **48**, 2308–2312.
18 Z. Sun, N. Zhang, Y. Si, S. Li, J. Wen, X. Zhu and H. Wang, *Chem. Commun.*, 2014, **50**, 9196–9199.
19 Y. Song, K. Qu, C. Zhao, J. Ren and X. Qu, *Adv. Mater.*, 2010, **22**, 2206–2210.
20 H. Wang, S. Li, Y. Si, Z. Sun, S. Li and Y. Lin, *J. Mater. Chem. B*, 2014, **2**, 4442–4448.
21 H. Wang, S. Li, Y. Si, N. Zhang, Z. Sun, H. Wu and Y. Lin, *Nanoscale*, 2014, **6**, 8107–8116.
22 Y. Song, X. Wang, C. Zhao, K. Qu, J. Ren and X. Qu, *Chem. – Eur. J.*, 2010, **16**, 3617–3621.
23 U. T. Bornscheuer, G. W. Huisman, R. J. Kazlauskas, S. Lutz, J. C. Moore and K. Robins, *Nature*, 2012, **485**, 185–194.
24 M. Mahmoudi, K. Azadmanesh, M. A. Shokrgozar and S. Laurent, *Chem. Rev.*, 2011, **111**, 3407–3432.
25 M. Valden, X. Lai, K. Luo, Q. Guo and D. W. Goodman, *Science*, 1998, **281**, 1647–1650.
26 X. Wang, Q. Wu, Z. Shan and Q. Huang, *Biosens. Bioelectron.*, 2011, **26**, 3614–3619.
27 S. Lee, C. Fan, T. Wu and S. L. Anderson, *J. Am. Chem. Soc.*, 2004, **126**, 5682–5683.
28 A. Asati, S. Santra, C. Kaittanis, S. Nath and J. M. Perez, *Angew. Chem., Int. Ed.*, 2009, **48**, 2308–2312.
29 Z. Liu, L. Tong and T. Zhu, *Chem. Soc. Rev.*, 2011, **40**, 1296–1304.
30 Y. Xia, C. M. Cobley, J. Chen and L. Wang, *Chem. Soc. Rev.*, 2011, **40**, 44–56.
31 J. P. Wilcoxon and B. L. Abrams, *Chem. Soc. Rev.*, 2006, **35**, 1162–1194.

32 W. Guo, J. Yuan, Q. Dong and E. Wang, *J. Am. Chem. Soc.*, 2010, **132**, 932–934.
33 S. Tanaka, J. Miyazaki, D. Tiwari and T. Jin, *Angew. Chem., Int. Ed.*, 2010, **49**, 1–6.
34 J. Sharma, H. C. Yeh, H. Yoo, J. H. Werner and J. S. Martinez, *Chem. Commun.*, 2011, **47**, 2294–2296.
35 Y. Tao, Y. Lin, Z. Huang, J. Ren and X. Qu, *Adv. Mater.*, 2013, **25**, 2594–2599.
36 J. Xie, Y. Zheng and J. Ying, *J. Am. Chem. Soc.*, 2009, **131**, 888–889.
37 N. Ma, A. F. Marshall and J. H. Rao, *J. Am. Chem. Soc.*, 2010, **132**, 6884–6885.
38 J. Xie, Y. Zheng and J. Ying, *Chem. Commun.*, 2010, **46**, 961–963.
39 T. Chen, Y. Hu, Y. Cen, X. Chu and Y. Lu, *J. Am. Chem. Soc.*, 2013, **135**, 11595–11602.
40 C. Guo and J. Irudayaraj, *Anal. Chem.*, 2011, **83**, 2883–2889.
41 Y. Wu, S. Chakrabortty, R. A. Gropeanu, J. Wilhelmi, Y. Xu, K. S. Er, S. L. Kuan, K. Koynov, Y. Chan and T. Weil, *J. Am. Chem. Soc.*, 2010, **132**, 5012–5014.
42 L. Zhang, S. Li, M. Dong, Y. Jiang, R. Li, S. Zhang, X. Lv, L. Chen and H. Wang, *Biosens. Bioelectron.*, 2017, **87**, 1036–1043.
43 J. Jun, H. Nguyen, S. Paik, H. Chun, B. Kang and S. Ko, *Food Chem.*, 2011, **127**, 1892–1898.
44 Y. Guo, L. Deng, J. Li, S. Guo, E. Wang and S. Dong, *ACS Nano*, 2011, **5**, 1282–1290.
45 K. Chattopadhyay and S. Mazumdar, *Biochemistry*, 1999, **39**, 363–370.
46 J. A. Nicel and H. Wright, *Enzyme Microb. Technol.*, 1997, **21**, 302–310.
47 Z. Lin, Y. Xiao, Y. Yin, W. Hu, W. Liu and H. Yang, *ACS Appl. Mater. Interfaces*, 2014, **6**, 10775–10782.
48 J. Xu, F. Shang, J. H. T. Luong, K. M. Razeeb and J. D. Glennon, *Biosens. Bioelectron.*, 2010, **25**, 1313–1318.
49 X. Zhao, Z. Mai, X. Kang and X. Zou, *Biosens. Bioelectron.*, 2008, **23**, 1032–1038.
50 J. Hu, Y. Yu, H. Guo, Z. Chen, A. Li, X. Feng, B. Xi and G. Hu, *J. Mater.Chem.*, 2011, **21**, 5352–5359.
51 Y. Wang, X. Bian, L. Liao, J. Zhu, K. Guo, J. Kong and B. Liu, *Microchim. Acta*, 2012, **178**, 277–283.
52 G. Zhao, Z. Yin, L. Zhang and X. Wei, *Electrochem. Commun.*, 2005, **7**, 256–260.
53 L. Hu, Y. Yuan, L. Zhang, J. Zhao, S. Majeed and G. Xu, *Anal. Chim. Acta*, 2013, **762**, 83–86.
54 F. Wen, Y. Dong, L. Feng, S. Wang, S. Zhang and X. Zhang, *Anal. Chem.*, 2011, **83**, 1193–1196.
55 Y. Liu, K. Ai, X. Cheng, L. Huo and L. Lu, *Adv. Funct. Mater.*, 2010, **20**, 951–956.
56 A. L. Sanford, S. W. Morton, K. L. Whitehouse, H. M. Oara, L. Z. Lugo-Morales, J. G. Roberts and L. A. Sombers, *Anal. Chem.*, 2010, **82**, 5205–5210.
57 L. Qu, Y. Liu, S. He, J. Chen, Y. Liang and H. Li, *Biosens. Bioelectron.*, 2016, **77**, 292–298.